


Hydrochemistry and quality of groundwater in alluvial aquifer of Karonga, Malawi

Harold Wilson Tumwitike Mapoma^{1,2}  · Xianjun Xie¹ · Yaqing Liu¹ · Yapeng Zhu¹ · Floney Patame Kawaye² · Tabitha Mlowoka Kayira²

Received: 28 August 2015 / Accepted: 20 April 2017 / Published online: 3 May 2017
© Springer-Verlag Berlin Heidelberg 2017

Abstract This study highlights the quality of groundwater for both drinking and irrigation in Karonga north where subsistence and commercial farming is practiced. All major groundwater quality descriptors and selected trace elements (iron, manganese, arsenic, and aluminum) were studied. The study demonstrated evidence of higher concentrations of bicarbonates (60–590 mg/L), total iron (2.2–5336 µg/L), total manganese (0.1–804 µg/L) and total arsenic (0.4–14.5 µg/L) in certain samples with low values of Eh (−32.0 to +25.8) and NO₃[−] (≤8.2 mg/L) against WHO standards. Thirty-six percent of samples were rated as poor using the water quality index (WQI) criteria. No scaling potential was observed using the Langelier analysis. The majority of samples were of the mixed-bicarbonate type with the abundance order of cations as Ca²⁺ > Na⁺ > Mg²⁺ > K⁺. Carbonate dissolution, silicate weathering and cation exchange were identified as possible main geochemical control mechanisms. The sources responsible for fluoride and nitrate include anthropogenic activities and rock–water interaction. Dissolution/precipitation and pH control the levels of As, Fe and Mn.

Keywords Groundwater · Hydrochemistry · Arsenic · Iron · Fluoride · Manganese · Karonga

✉ Harold Wilson Tumwitike Mapoma
hmapoma@poly.ac.mw

✉ Xianjun Xie
xjxie@cug.edu.cn

¹ School of Environmental Studies and State Key Laboratory of Biogeology and Environmental Geology, China University of Geosciences, 430074 Wuhan, China

² Department of Physics and Biochemical Sciences, University of Malawi, The Polytechnic, P/Bag 303, Blantyre 3, Malawi

Introduction

The significance of groundwater and the growing demand of the commodity for domestic and commercial use make it vulnerable to degradation. Water resource degradation is a serious issue that needs constant monitoring and assessment from an ecosystem perspective to human acceptability. The overarching issues of quality and health hazards related to groundwater are an area that continues to fascinate and stimulate scientific investigations and policy making everywhere around the world. It is true that primary production depends on both soil and water quality. In this regard, the physico-chemical quality of water and its availability affects crop production, crop quality and human health. In turn, this has repercussions on sustainable development at local, regional and global scale. Thus, assessment of physico-chemical parameters, evaluating the causes of variation in groundwater quality and prescribing the water quality indices are very crucial to managing water resources.

The groundwater chemical distribution is mainly determined by variations in aquifer geology. These variations are sometimes noted within short distances of the aquifer (Mapoma and Xie 2014; Mapoma et al. 2014). Soil used for crop production may be altered in its physical and chemical characteristics due to the water used for irrigation. For instance, irrigating land with sodic groundwater may elevate the sodicity of soils. Also, contaminated surface water used for irrigation and its return flow may infiltrate and contaminate groundwater.

Malawi's economy depends on agriculture. In most parts of the country (especially rural areas), agricultural activities depend on groundwater (Mapoma and Xie 2014; Mkandawire 2008). These activities demand good quality water ideal for crop production and animal husbandry.

Research on the suitability of groundwater for irrigation and drinking purposes has been done in various districts of Malawi (Mapoma and Xie 2014; Monjerezi and Ngonondo 2012; Monjerezi et al. 2011; Wanda et al. 2011, 2013). Despite including arsenic in some studies, all the studies in Malawi so far have identified that arsenic is below detectable limit or generalized the values to be below a certain threshold that is insignificant compared to the (WHO 2011) maximum allowable limit value (MALV) of 10 µg/L. While As has become a major topic of discussion across the globe, most of the papers find it interesting to present and discuss results that show significantly high levels in groundwater and evidence of arsenicosis cases. However, showing the presence of As in groundwater, albeit low, is important for groundwater quality management and decision making.

However, low doses due to presence of low arsenic over a prolonged period may affect human health. Also, such low available arsenic in groundwater used for irrigation or the bioavailable arsenic may accumulate/bioconcentrate in crops such as rice. Rice is believed to be much more efficient at accumulating arsenic into the grain than other staple foods (Bhattacharya et al. 2012; O'Neill et al. 2013; Rahmanian et al. 2015; Sun et al. 2008). Eating rice and drinking water that contains traces of arsenic over a long period of time can contribute to human health problems.

The selected study area is suitable for rice growing because the surface soil has a high water holding capacity. Generally, rice is grown in submerged flooded conditions. Often such conditions promote arsenic bioavailability for uptake through plant root system (Bhattacharya et al. 2012; O'Neill et al. 2013; Rahmanian et al. 2015; Sun et al. 2008). When the surface is flooded, gaseous exchange between atmosphere and the aquifer is impeded resulting in O₂ deficiency in the groundwater. This condition favors reductive dissolution processes which may mobilize arsenic and other toxic trace elements.

A study on the groundwater suitability for irrigation and drinking in Karonga was done in the past (Wanda et al. 2013). In their conclusion, the groundwater was pronounced to be fit for irrigation based on sodium adsorption ratio (SAR) and magnesium hazard (MH) values. However, Wanda et al. (2013) did not include iron (Fe), fluoride (F), manganese (Mn) and arsenic (As) in their study. In this study, Fe, F, Mn and As are included to provide additional insight into the groundwater quality in Karonga. This study evaluated the hydrochemical and quality of groundwater using water quality index (WQI). The geochemical controls on the variations in hydrochemistry were assessed using multivariate statistics' principal component analysis (PCA). PHREEQC modeling was used to explain the saturation state of groundwater with respect to the mineral phase.

Location of study area: economic, geologic and hydro-geological setting

Location, topography and economic activities

Karonga district is located in the northern region of Malawi sharing administrative boundaries with Rumphu (South), Chitipa (to the west) and international boundary with Tanzania (in the north and east) (Fig. 1a). The entire district covers an area of 3355 km² and a total population of 194,572 people. The town of Karonga (Fig. 1) is the center of local and international trade (mostly with Tanzania). It is located within latitudes -9.9972° to -9.9108° and between longitudes 33.8868° and 33.9372° . The average elevation of the town is 478 m above mean sea level (amsl).

Economically, cotton, rice and maize are the principal crops grown and sold in the eastern part of the district while coffee and livestock farming are practiced in the western part of Karonga. Subsistence to semi-commercial fishing is practiced throughout the district. In the study area, the central part of the district is dominated by cotton and maize production while the northern (across North Rukuru River) dominated by rice production. The discovery and subsequent mining of uranium in the Karoo deposits has bolstered economic development including replacement of graveled roads with tarmac (asphalt) roads (Wright et al. 2014). This has improved accessibility, increased human population and enhanced economic activities which in turn may put pressure on groundwater resources.

Climate and geology

Karonga district has a subtropical climate characterized by rainy season (November to May) and dry season (June to October). The average temperature of the district is $24.4 \pm 5.2^{\circ}\text{C}$ with a maximum annual rainfall of 799 mm.

The geology of Karonga is part of the Ubendian belt grouping (Chitipa–Karonga) comprising of several mafic–ultramafic bodies. The topography is characterized by a flat plain in the north and rolling plain in the southern part with mountains in the west. The bounding features are distinct of the East African Rift System (EARS). In the west, the Nyika Plateau rises from the rift valley (around 500 m) to 2500 m amsl. In the eastern margin, the surface elevation of the lake is around 500 m amsl (Wright et al. 2014).

The geomorphology of the area consists of Karoo sediments, Cretaceous–Pleistocene Sediments and Quaternary (alluvium) formations (Fig. 1b) overlaying the crystalline Basement complex of Precambrian to lower Paleozoic age. This Basement complex is distinguished by low grade

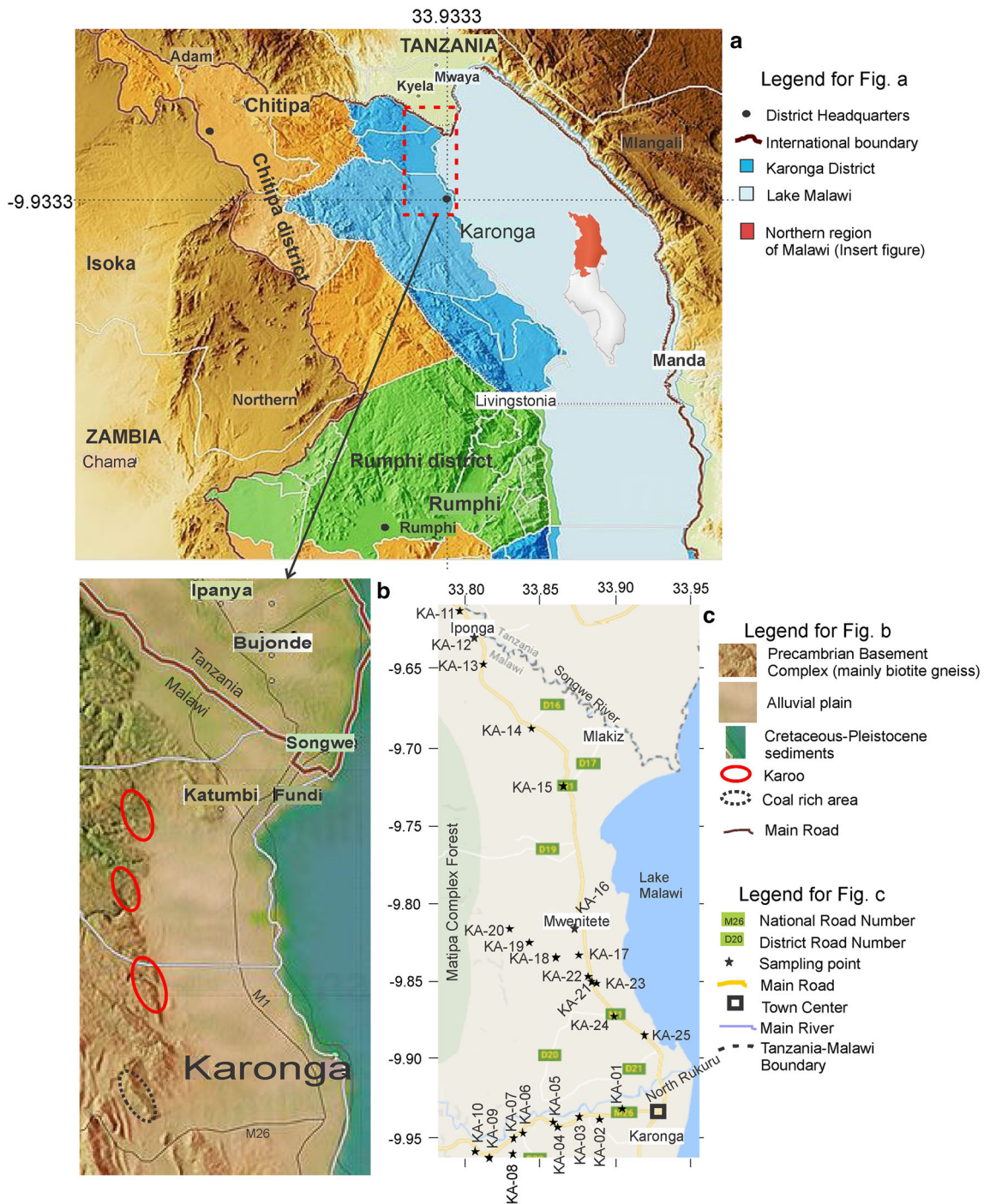


Fig. 1 Location of Karonga District in the Northern Region of Malawi (insert is map of Malawi showing the Northern Region) (a), the general geological features of the study area showing main lithological units, i.e., Precambrian Basement Complex and Alluvium

(the approximate location of Karoo deposits are circled) (b) and, map showing location of sampling points, the North Rukuru and Songwe Rivers (c) (base maps courtesy of Maphill, <http://www.maphill.com/search/karonga/>)

metamorphic gneisses (Mafingi group) belonging to amphibole facies (Chilton and Smith-Carington 1984; Dill et al. 2005). Karoo sediments are characterized by high content of coal seams resting on sandstones and argillaceous schist (Fagereng 2013; Macheyeke et al. 2015).

These sediments are well bonded by calcite and hardened. Therefore, they have low porosity and can reach over 3500 m thick.

Cretaceous–Pleistocene sediments are found in small narrow elongated patches, stretching parallel to the shores of

Lake Malawi (Fig. 1b). They include crumbly sandstones, unconsolidated sands, sandy marls, clays and conglomerates. These sediments are mainly sandstone formations of desert origin, with abundant traces of evaporites. The permeability and porosity of these rocks are probably high.

Quaternary formations (alluviums, colluviums, lacustral deposits) are well developed in the immediate vicinity of the lakeshore (Fig. 1b). They are consistent of lacustrine deposits probably remnants of periods of Lake Malawi withdrawal or residues of prehistoric water mass (Stephens 1966). The lithology consists of intersection of clays, silts, sands and gravels (Macheyeki et al. 2015; Thompson et al. 2012; Wright et al. 2014). The aquifers formed of fluvial and lacustral sediments are heterogeneous both vertically and horizontally.

Permeability of alluvial aquifers of Malawi is relatively high compared to weathered basement complex and furnishes better yield (Chilton and Smith-Carington 1984). The exact sampling area within the district (Fig. 1b, c) is bounded by hills to the west and Lake Malawi to the east, stretching from the Karonga-Chitipa road to Malawi-Tanzania border (the North Rukuru–Songwe Plain). The plain is dissected by rivers North Rukuru, Kibwe, Rufira, Kyungu and bounded by Songwe (north end of study area). General groundwater flow is from the western highlands toward the lake in the east. The recharge is mostly from high rainfall in the hills that contributes to lateral in-flow with infiltrating rainfall contributions. The aquifer in the region is semi-confined.

In recent years there has been a rise in groundwater demand that increased drilling of boreholes. The best groundwater yields in Karonga come from the alluvial aquifer and the littoral areas of the Lake (Chilton and Smith-Carington 1984; Chimphamba et al. 2009).

Materials and methods

Sampling and in situ measurements

Manually pumped boreholes were sampled in this study (total of 25 samples, Fig. 1c). The borehole depth records in the study area indicate a range between 35 and 60 m. The sampling and subsequent analysis took place in April 2015. The samples were filtered on site using 0.45 μm membranes. Twenty-five samples for cation analyses were stored in 50 ml polypropylene bottles and acidified to $\text{pH} \leq 2$ using 6 M HNO_3 . The other set of 25 samples for anion analysis were not acidified. The samples were immediately stored in a refrigerator at the Department of Physics and Biochemical Sciences of University of Malawi. Preliminary analyses included immediate in situ measurements of pH, temperature, electric conductivity

(EC), total dissolved solids (TDS), total hardness and turbidity using standard commercial meters. Bicarbonate (HCO_3) was analyzed in the Department of Physics and Biochemical Sciences' chemistry laboratory via APHA titration technique (Rice et al. 2012). Borehole site elevation and coordinates were measured using a portable hand held global positioning system (GPS).

Laboratory analysis

Chemical analysis of the samples was done at State Key Laboratory of Biogeology and Environmental Geology of China University of Geosciences (Wuhan) within 1 week of sampling. All cations, namely calcium (Ca^{2+}), magnesium (Mg^{2+}), potassium (K^+), sodium (Na^+), silica (Si), total iron (Fe_T), aluminum (Al^{3+}), total manganese (Mn_T) and total arsenic (As_T), were analyzed by inductively coupled plasma optical emission spectrometry (ICP-OES)(ICAP 6300, Thermo Scientific). The average analytical error for major and trace chemical constituents using ICP-OES is less than $\pm 5\%$. In contrast, major anions (chlorine, Cl^- and sulfate, SO_4^{2-}) as well as fluorides (F^-) and nitrates (NO_3^-) were determined by ion chromatography (IC) (Dionex ICS 1100) with a detection limit of 0.01 mg/L. The ionic balance error was computed, taking the relationship between the total cations and total anions for each groundwater sample. All groundwater samples used in this analysis (especially for confidence in PHREEQC modeling results) had an ionic balance error within $\pm 5\%$ (Table 1).

Data analysis and interpretation

The data obtained from laboratory analysis were used to analyze the quality of groundwater for both domestic (mainly drinking) and irrigation purposes. This was achieved by comparing the results obtained with World Health Organization guiding values (WHO 2011) and analyzing the water quality index (WQI) values. Various water quality indices have been proposed that prove useful to decision makers on water resource management. The water quality index (WQI) proposed by Tiwari and Mishra (1985) is a reliable, useful and efficient method for assessing and communicating the information on the overall quality of water (Asadi et al. 2007; Pradhan et al. 2001; Srivastava et al. 2011). It helps in deciding the suitability of water sources for its intended purposes. This WQI follows the formula:

$$\text{WQI} = \text{Antilog} \left[\sum_{n=1}^n W_n^n \log_{10} q_n \right] \quad (1)$$

where W_n = weight factor, calculated from the following equation

Table 1 In situ measurements, laboratory analysis data and statistical summary of Karonga samples pitched against the WHO drinking water standards (where available)

Sample ID	Elevation m (amsl)	Eh (mV)	pH	Temp (°C)	Turb (NTU)	EC (µS/cm)	TDS (mg/L)	TH (mg/L)	Ca ²⁺ (mg/L)	Mg ²⁺ (mg/L)	Na ⁺ (mg/L)
KA-01	496	15.8	6.2	28	bdl	480	238	113	29.9	9.3	11.0
KA-02	504	13.9	6.2	30	1.8	1533	589	319	94.7	20.1	26.6
KA-03	513	-16.8	6.6	29	4.8	1181	592	189	47.2	17.3	85.2
KA-04	516	-8.5	6.5	30	bdl	1575	790	366	88.3	35.4	88.5
KA-05	507	-32.0	7.1	29	bdl	1197	634	177	44.7	15.9	88.6
KA-06	525	-6.4	6.6	29	bdl	968	484	249	73.7	15.9	20.8
KA-07	533	-19.4	6.7	30	bdl	1378	689	327	100.7	18.5	38.7
KA-08	525	-30.9	6.9	29	bdl	1594	798	298	84.7	21.0	72.8
KA-09	534	-21.7	6.8	29	bdl	1696	850	283	97.8	9.5	100.1
KA-10	533	-13.3	6.6	29	bdl	1427	716	418	154.5	7.8	19.5
KA-11	512	-8.9	6.6	28	1.5	417	209	54	14.1	4.6	14.9
KA-12	515	-10.0	6.6	30	1.4	611	305	151	29.3	18.9	8.5
KA-13	527	-17.6	6.7	27	0.5	660	328	169	46.2	13.1	12.2
KA-14	501	-5.2	6.5	28	4.4	213	105	42	11.3	3.3	5.8
KA-15	503	7.5	6.4	29	0.3	533	279	120	37.9	6.3	11.5
KA-16	483	11.1	6.3	29	23	351	174	60	13.8	6.2	11.8
KA-17	501	21.6	6.0	29	1.9	334	167	48	11.2	4.9	11.4
KA-18	496	17.9	6.1	29	0.5	415	207	79	17.3	8.6	13.8
KA-19	496	-7.4	6.4	29	0.4	1004	498	200	60.7	11.7	33.6
KA-20	502	25.8	6.3	30	bdl	306	154	54	17.0	2.7	4.2
KA-21	487	-9.0	6.5	30	bdl	946	451	224	79.4	6.2	21.8
KA-22	486	-7.7	6.7	29	0.1	573	283	123	36.0	8.0	16.7
KA-23	489	-23.3	6.7	30	bdl	1043	518	229	73.8	10.8	37.1
KA-24	492	-3.5	6.6	30	bdl	410	205	79	20.1	7.0	13.1
KA-25	494	3.6	6.4	29	bdl	568	285	105	26.6	9.4	18.2
Min	483	-32.0	6.0	27.0	0.1	213	105	42	11.2	2.7	4.2
Max	534	25.8	7.1	30.0	23.0	1696	850	418	154.5	35.4	100.1
Mean	507	-5.0	6.5	29.1	3.4	856	422	179	52.4	11.7	31.5
SD		16.0	0.3	0.8	6.4	477	232	109	37.0	7.4	29.9
WHO			6-8.5		5	750	1000		200	50	200

Sample ID	K ⁺ (mg/L)	HCO ₃ ⁻ (mg/L)	SiO ₂ ⁻ (mg/L)	Cl ⁻ (mg/L)	SO ₄ ²⁻ (mg/L)	F ⁻ (mg/L)	NO ₃ ⁻ (mg/L)	Fe _T (µg/L)	Mn _T (µg/L)	As _T (µg/L)	Al ³⁺ (µg/L)	Ion balance error (%)
KA-01	1.2	162	16.8	3.1	bdl	1.0	bdl	441.9	262.0	5.5	6.6	-0.29
KA-02	5.4	370	30.6	15.8	15.4	0.9	1.4	bdl	1.6	8.9	2.6	4.30
KA-03	2.5	400	24.7	7.1	2.4	1.3	4.9	182.7	538.0	14.5	1.6	4.16
KA-04	1.2	550	24.7	26.0	20.6	1.0	bdl	5.5	401.0	4.3	0.7	4.52
KA-05	6.2	420	20.2	9.5	17.8	2.0	bdl	52.3	274.0	7.7	bdl	-0.54
KA-06	4.1	328	25.2	7.4	3.4	1.0	bdl	20.2	263.0	4.7	bdl	2.43
KA-07	6.6	480	25.8	11.4	1.8	0.8	1.7	2.2	299.0	10.7	2.2	0.65
KA-08	7.4	578	17.2	7.6	2.0	0.8	3.5	14.6	256.0	8.7	bdl	-2.73
KA-09	5.0	590	24.1	7.3	3.4	1.2	8.2	2.2	1.3	13.1	2.0	0.00
KA-10	2.0	495	21.8	4.0	1.5	0.8	4.9	bdl	0.1	5.2	bdl	4.94
KA-11	8.3	120	33.1	3.2	1.3	1.0	0.5	4.9	656.0	9.5	5.0	-4.92
KA-12	2.6	218	20.1	3.5	bdl	0.4	0.8	3417.0	282.0	6.3	bdl	-1.76
KA-13	3.0	225	21.5	3.1	1.5	0.4	bdl	1833.0	373.0	7.2	2.0	2.94
KA-14	1.1	60	18.1	5.1	bdl	0.3	3.1	289.4	109.0	8.5	1.3	-2.77

Table 1 continued

Sample ID	K ⁺ (mg/L)	HCO ₃ ⁻ (mg/L)	SiO ₂ ⁻ (mg/L)	Cl ⁻ (mg/L)	SO ₄ ²⁻ (mg/L)	F ⁻ (mg/L)	NO ₃ ⁻ (mg/L)	Fe _T (μg/L)	Mn _T (μg/L)	As _T (μg/L)	Al ³⁺ (μg/L)	Ion balance error (%)
KA-15	3.5	165	24.7	3.9	2.1	0.6	bdl	60.7	482.0	2.8	5.3	1.97
KA-16	3.9	102	21.9	8.0	3.1	0.3	0.9	129.2	804.0	9.2	bdl	-4.89
KA-17	2.8	86	16.6	4.2	1.9	0.3	0.7	95.4	39.8	2.7	0.3	-1.94
KA-18	1.6	129	27.7	4.1	bdl	0.5	bdl	2641.0	488.0	9.3	2.1	0.99
KA-19	2.5	344	24.8	2.5	bdl	0.8	0.6	31.8	452.3	4.5	bdl	-2.23
KA-20	1.1	68	47.9	5.9	2.6	0.3	bdl	5.9	11.5	2.5	bdl	-2.89
KA-21	2.8	308	23.1	2.8	bdl	0.5	bdl	7.4	423.0	10.5	bdl	3.18
KA-22	1.7	184	20.4	5.7	2.2	0.4	bdl	190.8	221.0	7.5	bdl	-0.34
KA-23	4.7	350	24.3	2.9	2.3	0.3	3.3	35.5	171.0	8.3	bdl	3.02
KA-24	1.7	130	24.1	3.8	2.2	0.4	bdl	991.4	151.0	8.2	5.1	-1.74
KA-25	1.7	180	26.9	3.0	bdl	0.6	bdl	5336.0	373.0	0.4	6.1	0.93
Min	1.1	60	16.6	2.5	1.3	0.3	0.5	2.2	0.1	0.4	0.3	-4.9
Max	8.3	590	47.9	26.0	20.6	2.0	8.2	5336.0	804.0	14.5	6.6	4.9
Mean	3.4	282	24.3	6.4	4.9	0.7	2.7	686.6	293.3	7.2	3.1	0.3
SD	2.1	169	6.4	5.2	6.1	0.4	2.3	1365.3	211.2	3.4	2.1	
WHO	100	250		600	400	1.5	50.0	1500.0	400.0	10.0		

Amsl, above mean seas level; bold, exceeding WHO maximum allowable limit value; bdl, below detection limit, Temp, temperature; Turb, turbidity

$$W_n = K(S_i)^{-1}$$

with K the proportionality constant derived from

$$K = \left[\sum_{i=1}^n (S_i)^{-1} \right]$$

Here, S_i values are the standard values of the water quality parameter (WHO 2011).

Quality rating (q_n) was calculated using the formula

$$q_n = \left[\frac{V_{\text{actual}} - V_{\text{ideal}}}{V_{\text{standard}} - V_{\text{ideal}}} \right] \times 100$$

where q_n is quality rating of i th parameter for a total of n water quality parameters, V_{actual} is the value of the water quality parameter obtained from laboratory analysis, V_{ideal} is the value of that water quality parameter that can be obtained from the standard tables, V_{ideal} for pH = 7 and for other parameters is equivalent to zero, and V_{standard} is the standard of the water quality as prescribed by WHO (2011).

The calculated WQI values are then used to rate the groundwater quality as excellent, good, poor, very poor and unfit for human consumption (Table 2).

Indicators of irrigation quality were assessed using sodium adsorption ratio as follows:

$$\text{SAR} = \frac{[\text{Na}^+]}{\sqrt{[\text{Ca}^{2+}] + [\text{Mg}^{2+}]}} \quad (2)$$

where the ionic concentrations are in mmol/L.

The computed SAR values and field EC data were used to explain the suitability of groundwater for irrigation using Wilcox diagram. Also, the Langelier Saturation Index (LSI) was computed using Aquachem 2011.1 to evaluate scaling potential of groundwater in the area. A piper plot was used to summarize the general groundwater hydrochemical facies.

The geochemical modeling was done using PHREEQC version 3.0 (Parkhurst and Appelo 1999), implemented with MINTEQ.v4 database (Allison et al. 1991) while the interrelationship among the hydrochemical elements was assessed using SYSTAT's principal component analysis (PCA).

Results and discussion

General physical–chemical and irrigation quality of groundwater

The physico-chemical results and summary statistics for all 25 samples are listed in Table 1. In the same table, WHO (2011) standards for drinking water are included to guide on the general water quality. Compared with WHO limit values for drinking water, all major groundwater quality descriptors, except for HCO₃⁻ (48% exceedance), were within range acceptable for human consumption (Table 1). Cases of higher values than WHO threshold limit for Fe_T, Mn_T and As_T were observed as highlighted in Table 1.

Table 2 Water types for each sample acquired from AquaChem 2011.1 and the water quality index computed using Ms Excel

Sample ID	Location name	Water type	WQI	Quality	Probable reason (Table 1)
KA-01	Lukulu Primary	Ca–Mg–HCO ₃	55.07	Poor	
KA-02	Diocece Primary	Ca–Mg–HCO ₃	75.70	Very poor	High HCO ₃ ⁻
KA-03	Mwakwama 2	Na–Ca–HCO ₃	141.60	Unfit for drinking	High HCO ₃ ⁻ , Mn _T , As _T and turb
KA-04	KIP 16 Lasha 2	Ca–Na–Mg–HCO ₃	42.70	Good	
KA-05	KIP 138 Lasha 1	Na–Ca–HCO ₃	75.47	Very poor	High HCO ₃ ⁻ and F ⁻
KA-06	KIP 003 Murwa	Ca–Mg–HCO ₃	46.39	Good	
KA-07	Mbande School KK139	Ca–Na–HCO ₃	100.97	Unfit for drinking	High HCO ₃ ⁻ and As _T
KA-08	Mwenenguwe/PM481	Ca–Na–HCO ₃	83.32	Very poor	High HCO ₃ ⁻
KA-09	Ngemera 1 CDC/01/91	Ca–Na–HCO ₃	107.86	Unfit for drinking	High HCO ₃ ⁻ , As _T and Na ⁺
KA-10	Khande TDC/KIP134	Ca–HCO ₃	42.17	Good	
KA-11	Ndenga 1 CDC/01/069	Ca–Na–HCO ₃	92.37	Very poor	High Fe _T
KA-12	Timoti Irrigation	Mg–Ca–HCO ₃	63.27	Poor	
KA-13	Iponga T. Center	Ca–Mg–HCO ₃	72.07	Poor	
KA-14	Mwangulukulu Cattle Dip Tank	Ca–Mg–Na–HCO ₃	81.06	Very poor	High Turb and low TDS
KA-15	Ighembe School	Ca–HCO ₃	28.72	Good	
KA-16	Mwenitete Primary School	Ca–Na–Mg–HCO ₃	91.37	Very poor	High Mn _T and Turbidity
KA-17	Shaliso	Ca–Na–Mg–HCO ₃	26.08	Good	
KA-18	Kakoma School CDC/09/002	Ca–Mg–Na–HCO ₃	93.30	Very poor	High Fe _T and Mn _T
KA-19	Mwangomba/Mwamulima	Ca–Na–HCO ₃	45.17	Good	
KA-20	Ngerenge CDSS	Ca–HCO ₃	23.12	Excellent	
KA-21	Fundi 1	Ca–HCO ₃	100.56	unfit for drinking	High HCO ₃ ⁻ , Mn _T and As _T
KA-22	Fundi 2 CDC/KA/007	Ca–Na–Mg–HCO ₃	73.02	Poor	
KA-23	Tchowo School CDC 08	Ca–Na–HCO ₃	78.94	Very poor	High HCO ₃ ⁻ and As _T
KA-24	Lusako School	Ca–Mg–Na–HCO ₃	79.64	Very poor	High Fe _T
KA-25	Malungo School KA/04	Ca–Na–Mg–HCO ₃	4.53	Excellent	

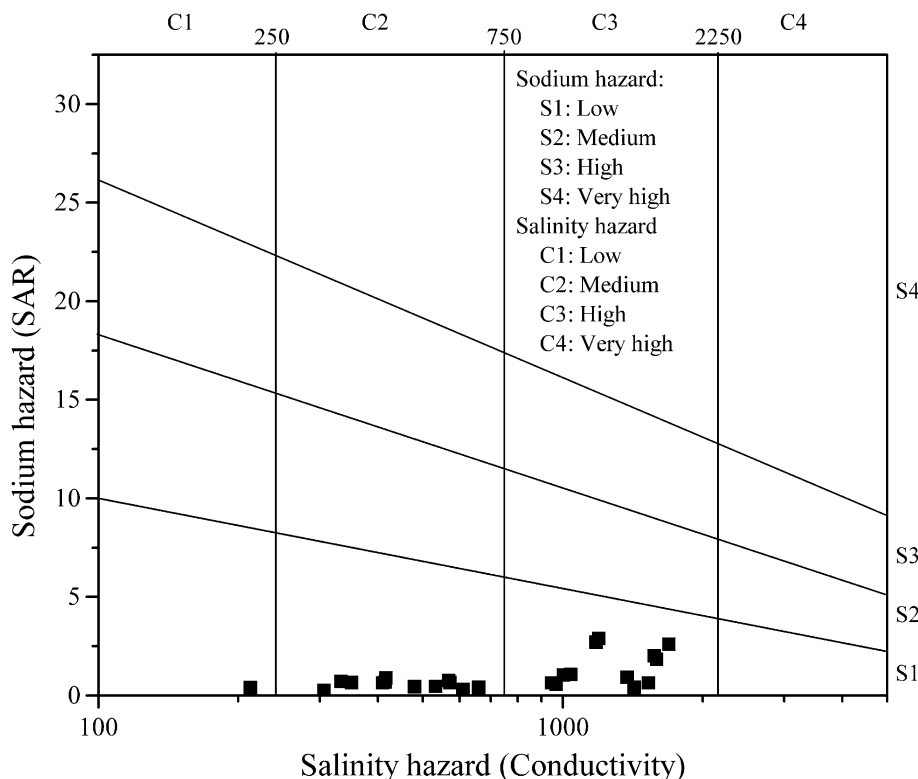
High alkalinity values were observed in the groundwater studied (Table 1). Although high alkalinity is synonymous with high pH, hardness and TDS values (Ayedun et al. 2011), the observed values for pH and TDS are lower than the maximum allowable limit values (MALV) (WHO 2011). The TDS and EC values obtained in this study are within the range identified in a past study done in the district (Wanda et al. 2013).

The absence of NO₃⁻ in 48% of the samples and low concentrations in the rest suggest either little influence from anthropogenic contamination (from low use of N-containing fertilizers) or poor amount of dissolved oxygen in the aquifer. In case of poor oxygen availability, nitrate reducing bacteria may be using NO₃⁻ as oxygen donor during organic matter degradation thereby reducing NO₃⁻ to NH₄⁺ (Merkel and Planer-Friedrich 2005). This phenomenon can equally apply to the observed low concentrations of SO₄²⁻ (and absent in 28% of samples) suggesting reduction of sulfate to sulfide and subsequent formation of sulfide minerals (Burton et al. 2013a, b). If gypsum availability is low in the aquifer (discussed later in this paper), it could be another reason for the low concentration of SO₄²⁻ observed. Fluoride and Al³⁺ were

below MALV (WHO 2011), except in one sample (KA-05) where F exceeded the 1.5 mg/L standard value (Table 1). Fluoride in groundwater is controlled by pH, availability of the F-mineral bearing rock (e.g., fluorite) and availability of complexing agents (Gomez et al. 2009; Rafique et al. 2009; Wang et al. 2009). Sixteen percent of samples showed values of arsenic above 10 µg/L standard value. The values are relatively lower than most of the cases reported in the arsenic laden areas of the world (Smedley and Kinniburgh 2002). However, further investigation and follow-ups are recommended to completely certify that the situation is not hazardous to human health.

Table 2 provides information obtained using WQI analysis. In this table, most of the samples were rated poor for drinking. 36% of the samples were rated as very poor while 16% of the samples were unfit for drinking. However, this analysis used strict WHO standards for drinking water. The less stringent Malawi Standards Board (MSB 2005) may prove otherwise. The possible reasons for the observed quality rating in Table 2 are provided in the last column. This table may assist water quality managers/assessors in the district to make proper decisions pertaining to groundwater quality and use.

Fig. 2 Wilcox diagram illustrating the quality of groundwater fitness for irrigation in Karonga north based on SAR and salinity hazard criteria (C1–S1 sample is KA-14 while C3–S1 group contains KA-02, KA-03, KA-04, KA-05, KA-06, KA-07, KA-09, KA-10, KA-11, KA-19, KA-21 and KA-23 and the rest falling under C2-S1)



The Wilcox diagram (Fig. 2) relates sodium adsorption ratio (SAR), which expresses the sodium or alkali hazard to EC (a salinity hazard). The low sodium hazard (SAR) values (Fig. 2) indicate that the groundwater in this aquifer is suitable for irrigation farming. However, the salinity hazard ranges from low (C1, KA-14), medium (C2, 48% of total samples) and High (C3, 48% of total samples) (Fig. 2). C2-S1 is a medium salinity hazard and low sodium hazard groundwater category that can be used for irrigation if moderate amount of leaching occurs and with little danger for development of harmful levels of exchangeable sodium. Plants with moderate salt tolerance including maize and most crops and fruits grown in the district can thrive on C2-S1 water without worrying over salinity management (Etteieb et al. 2015; Zouahri et al. 2015). A high salinity hazard and low sodium hazard (C3-S1) observed in 48% of samples suggest that the groundwater is not ideal for use on soils with restricted drainage. But there is little danger for the development of harmful levels of exchangeable sodium (Etteieb et al. 2015; Wanda et al. 2013). In terms of magnesium hazard, only one sample (KA-12) showed a value higher than 50% (MH = 51.1%). This is the only sample whose Mg^{2+} values predominated that of Ca^{2+} and Na^+ (See next section on water types). A high MH value relative to Ca^{2+} may cause soils to become more alkaline that can affecting crop production. In terms of scaling potential in pipeline, the groundwater was undersaturated with respect to

calcium carbonate, according to the Langelier Saturation Index observed (LSI = -4.31 to -2.60). The undersaturated water has a tendency to remove existing calcium carbonate protective coatings in pipelines and equipment thereby abating the scale formation (Singh et al. 2006).

Figure 3 suggests a dominance order of major cations as follows: $Ca^{2+} > Na^+ > Mg^{2+} > K^+$. Typically, alkaline earths are expected to significantly exceed the alkali in the basement complex of Malawi (Mapoma et al. 2014; Wanda

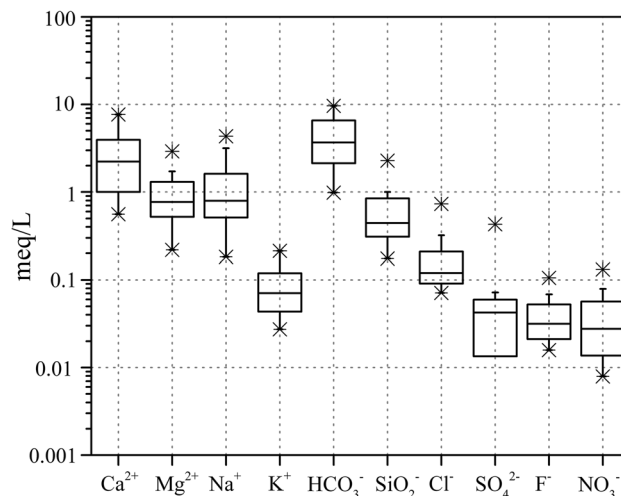


Fig. 3 Variations of major chemical constituents of groundwater investigated in Karonga north

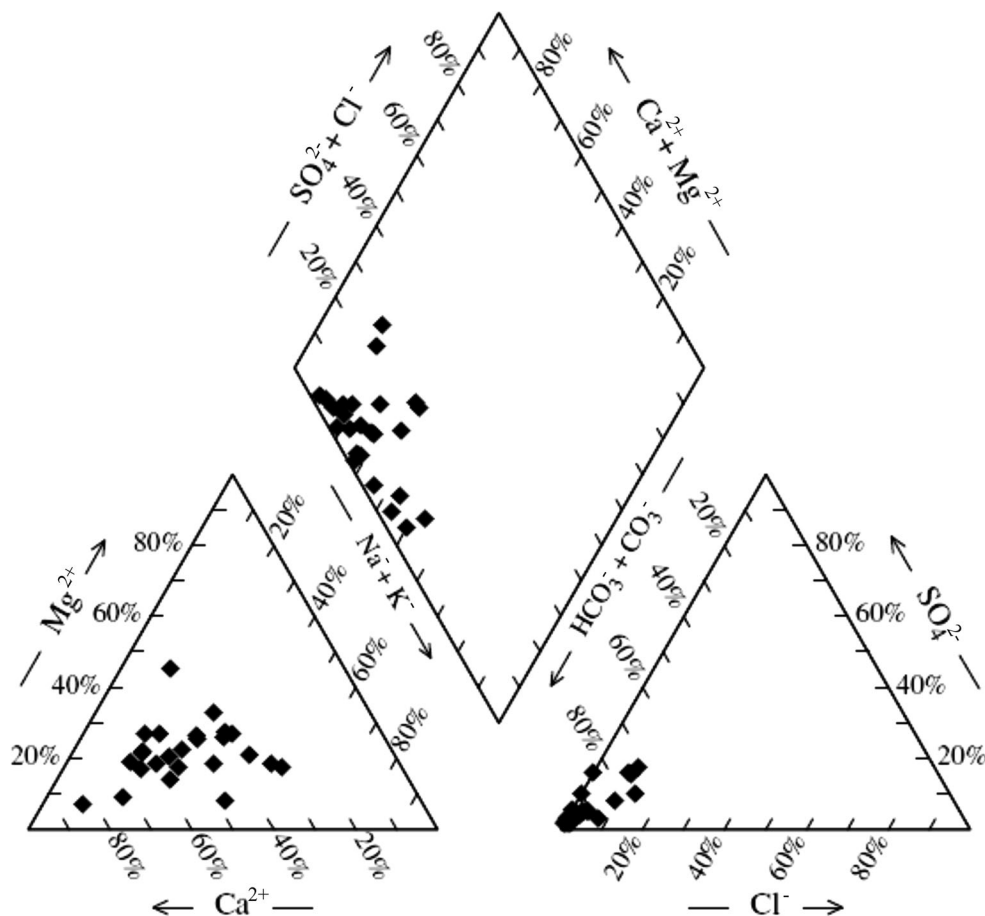
et al. 2013). In this study, though the alluvial plain is underlain by the basement complex (where the alkaline earths exceed the alkalis), Na^+ exceeded Mg^{2+} levels. It is known that heterogeneities in aquifer mineralogy may occur within short distances, which in turn affects the distribution of ions in the groundwater. Besides, the host rock mineralogy, other mechanisms such as cation exchange can affect the distribution whereby Na^+ may or may not exceed the alkaline earths. The HCO_3^- was the dominant anion observed in the system. A similar observation was noted in a previous study (Wanda et al. 2013). An increased level of SiO_2 over Cl^- and SO_4^{2-} suggests silicate weathering as a significant process over evaporite dissolution. As noted earlier, the basement complex is characterized by significant silicate minerals (Chilton and Smith-Carington 1984) whose weathering and deposition products constitute the alluvial plain aquifers in Malawi.

Spatial distribution of hydrochemical facies

To identify the groundwater type, a piper plot is presented (Fig. 4). Twenty-four percent (majority) of the groundwater samples were of the Ca-Na-HCO_3 type and 20% were of the Ca-Na-Mg-HCO_3 type (Table 2). As explained

earlier, the diversity in water type may be due to aquifer heterogeneity. The Ca-Na-HCO_3 and Ca-Na-Mg-HCO_3 water type may result from many processes including silicate weathering, carbonate dissolution, cation exchange, anaerobic degradation of organic matter and proton exchange. However, carbonate dissolution (calcite and dolomite) may control the Ca-HCO_3 and Ca-Mg-HCO_3 water type identified in this groundwater. Hence, the water type seems to suggest that the processes involving evaporite dissolution and mixing of recharge water with water from surface contamination sources such as fertilizers, irrigation return flows, domestic wastewater effluent and latrines (pit) are minimal. But, the presence of SO_4^{2-} , F^- , NO_3^- holds the fact that combination of evaporite dissolution and mixing of recharge water may contribute to the hydrochemical assemblage observed. A general spatial analysis shows a decrease in TDS transecting west to east of the study area (Fig. 5). However, the iso-contours display a distinct pattern of higher TDS values in southern part of the study area decreasing when moving northwards (Fig. 5). Samples in the southern part were taken parallel and close to North Rukuru River. The apparent flow dynamics of the river may trickle down its nutrients into the aquifer below, especially that the river carries large

Fig. 4 Piper diagram used to summarize the groundwater facies in the study area drawn using AqQa Version 1.1.1



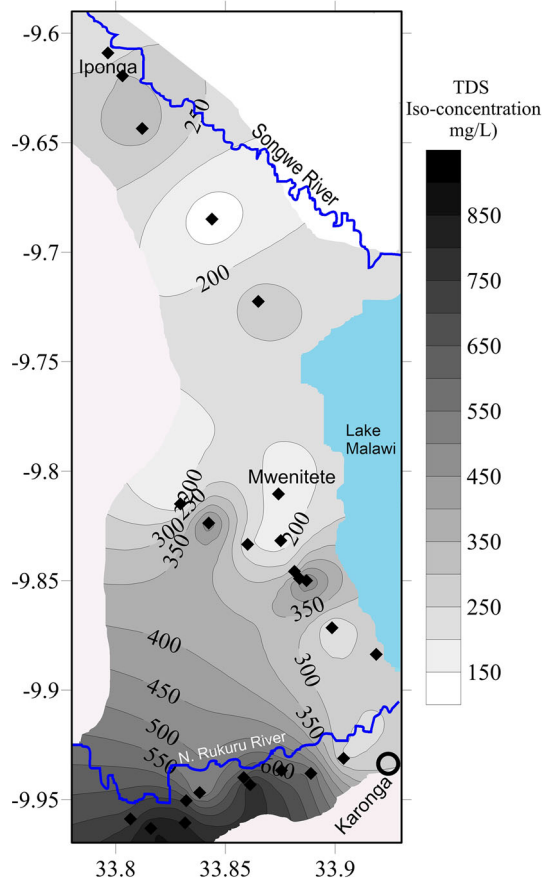


Fig. 5 Iso-concentration map showing the variations in TDS (mg/L) drawn using Kriging method in Surfer 11 software. The map includes main drainage, sampling points and names of main trading posts (Karonga, Mwenitete and Iponga)

volumes of detrital material and inorganic substances from far in the mountains (western margin) during rainy season.

The flow of groundwater in this area is slower than that of the highlands (weathered basement) as such, dissolution, desorption and rock–water interaction may be enhanced. Also, the areas in higher grounds are more aerated promoting oxidation processes unlike in this area.

Geochemical processes and groundwater evolution

The groundwater types observed and the variation in major cations/anions in the groundwater suggest a combination of mechanisms responsible for the geochemical processes occurring in the aquifer. Dominance of HCO_3^- suggests carbonate dissolution, organic matter decomposition and probably atmospheric influence on $\text{CO}_2(\text{g})$ dissolution as some of the processes responsible for observed hydrochemical distribution. Abundance of Na^+ may signify that cation exchange and halite dissolution are plausible while presence of significant SiO_2 suggests dissolution/weathering of silicate minerals such as pure or aluminosilicates end

members (Merkel and Planer-Friedrich 2005). Figure 6 suggests the mechanisms controlling the hydrochemistry of the studied groundwater while the saturation indices (Fig. 7) support the discussion.

Carbonate dissolution, silicate weathering and evaporite dissolution were investigated using a bivariate plot (Fig. 6a) (Halim et al. 2010; Mukherjee and Fryar 2008). The normalized Mg^{2+} versus Ca^{2+} shows that Mg^{2+} is mostly influenced by both carbonate dissolution and silicate weathering as the plots scatter in the region of silicate weathering-carbonate dissolution. Thus, aluminosilicates such as montmorillonite, silicates (e.g., sepiolite) and carbonates (dolomite, huntite and magnesite) are responsible minerals for presence of Mg^{2+} . After all, PHREEQC saturation indices show undersaturation of carbonate end members (dolomite, magnesite) (Fig. 7a) and silicates (chrysotile and sepiolite) (Fig. 7b). The model confirms that the dissolution of carbonates and silicates is responsible for the levels observed. The modeling results did not produce values for aluminosilicates that would have been responsible for Mg^{2+} levels.

Similarly, a plot of normalized HCO_3^- versus Ca^{2+} (Fig. 6b) show that elevated Ca^{2+} in the system is mostly from carbonate dissolution and probable silicate weathering (Halim et al. 2010; Mukherjee and Fryar 2008). In fact, the modeled saturation indices only confirmed the undersaturation of aragonite, calcite and dolomite minerals responsible for Ca^{2+} and HCO_3^- control in groundwater. But, as pH progresses toward neutral, the carbonate minerals (aragonite, calcite and dolomite) approach equilibrium with the liquid phase (Fig. 7c). Carbonate dissolution is limited above neutral pH due to constrain on $\text{CO}_2(\text{g})$ activity (Mapoma et al. 2014). Therefore, carbonate dissolution is responsible for the alkalinity, Ca^{2+} and Mg^{2+} observed in the groundwater. A study done in Karonga by Wanda et al. (2013) shows that about 28 and 36% of samples were undersaturated with respect to calcite and dolomite, respectively. In this study all samples were undersaturated with respect to these minerals. The deviation from Wanda et al. (2013) results may be due to differences in sampling period (as they sampled in both wet and dry season of 2011), and the samples were taken from a larger area than the present study representing high contrasting geological characteristics of the aquifer. More so, their results did not pinpoint the actual sampling points (geocodes not available) to validate our findings.

Though the assessment (Fig. 6a, b) shows that carbonate and silicate weathering are main mechanisms for Ca^{2+} and Mg^{2+} levels, the undersaturation of evaporites such as anhydrite, fluorite, gypsum (Fig. 7c) and in some instances ferromagnesians (e.g., magnesioferrite) (Fig. 7d) elevate Ca^{2+} and Mg^{2+} , respectively.

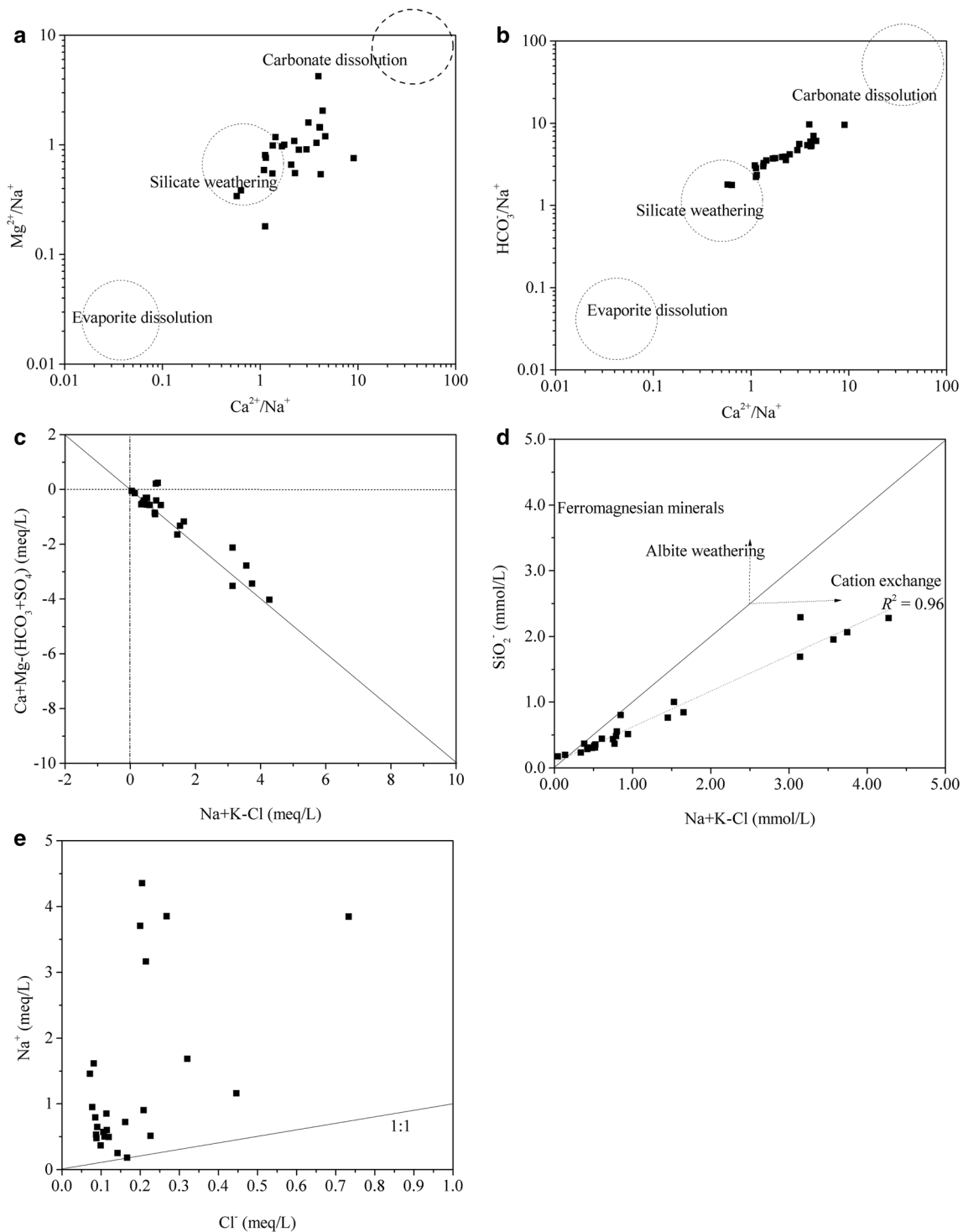


Fig. 6 Plot of normalized Mg^{2+} versus Ca^{2+} (a) and HCO_3^- versus Ca^{2+} (b) illustrating the predominant control mechanism. The assessment of significance of cation exchange (c), dominance of

cation exchange over albite and ferromagnesian sources of Na^+ (d) and possibility of halite dissolution (e)

The equivalent bivariate plot of normalized divalent cations versus corrected monovalent cations was used to evaluate the implication of cation exchange in the system (Fig. 6c). The deduction of anions (SO_4^{2-} and HCO_3^-)

from the divalent cations is necessary to correct the concentration that would otherwise have been realized from other processes than that of cation exchange. Such other processes include carbonate dissolution, silicate weathering

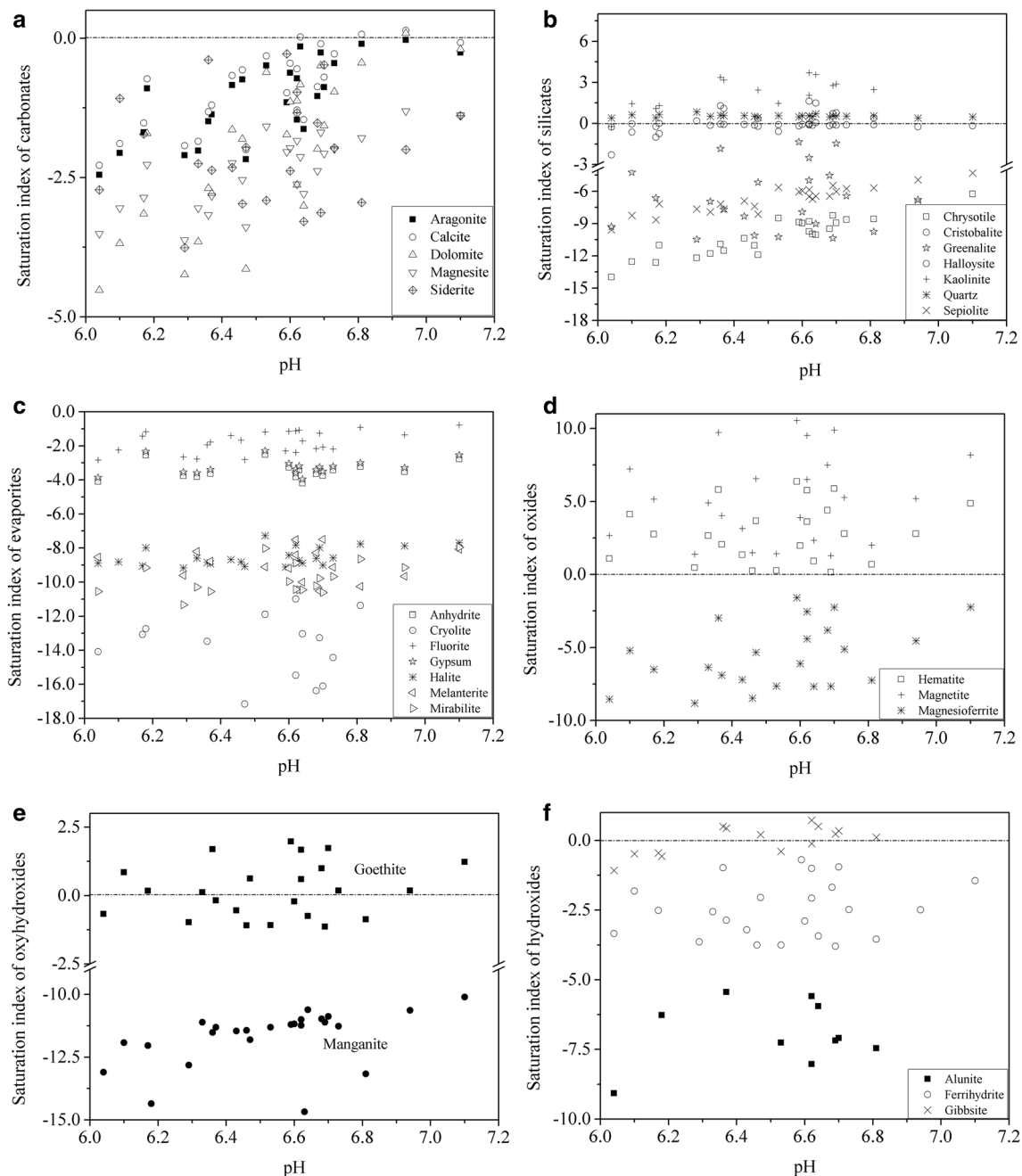
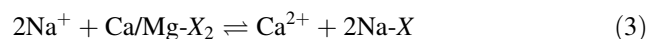
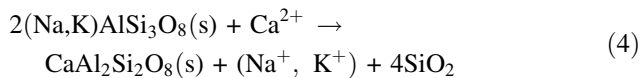


Fig. 7 PHREEQC modeled saturation indices for carbonates (a), silicates (b), evaporites (c), oxides (d), oxyhydroxides (e) and hydroxides (f) plotted against pH evolution

and evaporite (e.g., gypsum) dissolution (Kortatsi et al. 2008). The same procedure was applied to Na + K by removing interference of evaporites such as halite and silicate weathering. The regression slope (-0.85) strongly suggests that cation exchange between divalents and monovalent cations exists in the groundwater of the North Rukuru–Songwe alluvial aquifer as it is close to -1 (Mukherjee et al. 2009). Presence of clay minerals (e.g., sepiolite) may provide the available exchangers following Eq. (3), where X represents clay, such as:



In the reverse reaction (Eq. 3), the divalent cation is exchanged with Na^+ in the clay mineral to elevate Na^+ in the system. Similar scenario may apply for K^+ exchange with divalent cations from aluminosilicates, such as the exchange that may occur for an orthoclase ($(\text{Na}, \text{K})\text{AlSi}_3\text{O}_8$) of the feldspar family to produce anorthite ($\text{CaAl}_2\text{Si}_2\text{O}_8$) releasing Na^+ and K^+ as shown in Eq. (4) below.



The samples in Fig. 6c plot in the fourth quadrant (negative ordinate and positive abscissa) suggesting enrichment of Na⁺ relative to Mg²⁺ (and Ca²⁺) (Monjerezi and Ngongondo 2012). Also, the regression analysis of SiO₂ versus Na + K – Cl shows that the strong positive relationship (Fig. 6d) falls in the cation exchange region as opposed to weathering of silicates (e.g., albite) and ferromagnesian dissolution (Mukherjee and Fryar 2008). This confirms that Na + K levels are controlled mostly by cation exchange. Generally, the regression shows that as Na + K – Cl increases, SiO₂ increases linearly implying that Na + K is indeed from aluminosilicates but due to cation exchange process with divalent cations. In support of this, the levels of SiO₂ produced from cation exchange are buffered by the equilibrium state of water with pure silicates such as cristobalite and quartz (Fig. 7b). Furthermore, it is deduced that halite dissolution is not the main source of elevated Na⁺ (Fig. 6e) as the plots scatter significantly away from the halite dissolution line (Halim et al. 2010; Yidana 2010). Cation exchange and to a certain extent silicate weathering are more responsible for Na⁺ and K⁺ levels.

Infiltrating water from the surface that accumulated evaporites during inundation periods of rice growing season may contribute Na⁺ levels in groundwater. The surface accumulated salts may dissolve and be introduced into groundwater through infiltrating water. Use of inorganic and organic fertilizer may be responsible for NO₃⁻ in the system (Yidana 2010). After all, it is shown that the liquid phase is undersaturated with respect to all evaporites (Fig. 7c) implying dissolution of these minerals to establish equilibrium. Such dissolution could contribute to Na⁺, K⁺, F⁻, Cl⁻ and SO₄²⁻ levels. But, the correlation between Ca²⁺ and SO₄²⁻ was poor (R² = 0.04, p > 0.05) thereby discounting gypsum dissolution as a source of SO₄²⁻. And, this study has already ruled out the significance of halite dissolution (Fig. 6e).

Principal component analysis (PCA)

Besides general interrelationships among parameters, the discussion in this section emphasizes on fluoride, nitrate, arsenic and manganese. The principal component analysis yielded 4 significant principal components (factor loadings) based on eigenvalue ≥ 1 and their high cumulative variance of 96.4%. The results are shown in Table 3.

The first factor which accounts for 29.3% of the total variance is characterized by very high loadings of EC, TDS, Na⁺, HCO₃⁻, SiO₂⁻, SO₄²⁻, F⁻, NO₃⁻ and moderate to high loadings of As_T. In this PC1 significant, but

Table 3 A SYSTAT rotated principal component matrix normalized using Varimax showing the five principal factors

	PC1	PC2	PC3	PC4
Eh	-0.376	-0.411	-0.049	-0.817
pH	0.341	0.308	0.128	0.841
Temperature	0.168	0.902	0.27	-0.239
Turbidity	-0.073	-0.300	-0.886	0.076
EC	0.668	0.662	0.200	0.274
TDS	0.666	0.664	0.196	0.275
TH	0.439	0.813	0.278	0.243
Ca²⁺	0.458	0.761	0.332	0.223
Mg²⁺	0.262	0.831	0.009	0.265
Na⁺	0.919	0.310	0.025	0.232
K⁺	-0.141	0.034	0.880	0.444
HCO₃⁻	0.671	0.639	0.255	0.267
SiO₂⁻	0.905	0.348	0.027	0.235
Cl⁻	0.121	0.973	0.063	0.172
SO₄²⁻	0.847	0.246	0.430	-0.124
F⁻	0.673	0.111	0.250	0.600
NO₃⁻	0.883	0.140	-0.210	0.195
Fe_T	-0.160	-0.178	-0.968	-0.067
Mn_T	-0.160	-0.178	-0.968	-0.067
As_T	0.565	0.296	-0.116	0.758
Al³⁺	-0.178	-0.327	0.539	0.749
Variance explained	6.150	5.900	4.457	3.731
% variance	29.288	28.096	21.225	17.769

Bold values indicate highest significant factor loadings for the physical-chemical parameters that explain the strong relationship among variables within a principal component

rather low, loadings of TH and Ca²⁺ are also indicated. This factor reveals traits of evaporite dissolution and contribution of the same to EC and TDS. It further explains the possibility of silicate weathering as a source of Na⁺ and that of F⁻ and NO₃⁻. Silicate weathering can have effect on mobilization of arsenic as well. Groundwater quality and the observed water facies are explained by PC2 which indicates high loadings of EC, TDS, TH, Ca²⁺, Mg²⁺, HCO₃⁻, Cl⁻ and accounted for 28.1% of total variance. As indicated earlier, HCO₃⁻ predominates in the anion group followed by Cl⁻. It further reveals that the EC and TDS values are contributed by the major groundwater cations and anions and that carbonate dissolution is more pronounced in the system. The third factor accounting for 21.3% of the total variance is associated with high negative loading of turbidity, Fe_T, Mn_T and positive loading of K⁺. A moderately negative loading of Al³⁺ is also observed in this factor. However, 14 out of 25 samples did not show any signs of turbidity. Mostly, the factor explains relationship of Fe_T and Mn_T that in part may contribute to the observed turbidity in some samples (Table 3). The high loading of K⁺ and moderate loading of Al³⁺ can explain

the importance of aluminosilicates that can probably contribute to K^+ and Al^{3+} in the samples. PC4 explains the relationship between the nature of groundwater (reduction potential and pH) and trace elements, especially Al^{3+} and As_T .

Fluoride and nitrate

Both elements are explained by PC1. This factor suggests that F^- may come from carbonate dissolution, evaporite sources and human activities. Presumable source of F^- in groundwater is dissolution of fluorite (CaF_2) (Rafique et al. 2008, 2009) as the saturation index (Fig. 7c) suggests dissolution of fluorite in the system. However, the relationship between Ca^{2+} and F^- is weak (though significant) as can be observed from the PCA and the Pearson's correlation coefficient ($r = 0.33$, $p = 0.54$). Although the groundwater contains higher levels of Ca compared to other cations, the dissolution of fluorite is not the only source of elevated fluoride in the groundwater of Karonga. Moreover, PC1 suggests that hydrolysis of alkali-F-rich minerals is a viable source. After all, the correlation coefficient for F^- versus Na^+ was significant ($r = 0.73$, $p < 0.001$). From the saturation indices, the groundwater is undersaturated with respect to cryolite (Na_3AlF_6) (Fig. 7c). The other F-minerals, such as silicate end members present in basement complex, can undergo hydrolysis to provide dissolved F^- (Wang et al. 2004). Therefore, dissolution of both fluorite and F-bearing minerals is the source of fluoride in the study area. Availability of complexing agents can affect the presence of fluoride as well (Wang et al. 2009).

Past records show up to 8 mg/L of fluoride detected in Karonga (Carter and Bennett 1973). This study had a maximum of 2 mg/L of F^- which is lower than that recorded in literature for Karonga. Several reasons may be attributed to the significant difference such as spatial-temporal hydrodynamics and seasonal variations. This study was conducted in rainy-rice growing season where the groundwater table should probably be higher than the dry season which might have diluted F^- levels. Otherwise, a follow-up study in dry season is needed. Also, it was not possible to obtain a sample from the exact water point that was studied in the area that produced the classic 8 mg/L F^- value and mimic the conditions, sampling procedure and analytical protocol that existed then. This remains unresolved as of now.

Despite the values obtained, fluoride in the right amounts is crucial to human health. Higher than threshold values is detrimental to human health. Lower than the required amount needs to be improved to safeguard human health. Dental fluorosis has been observed in some parts of the district but a study to assess the extent has not been

carried out yet owing to the low F^- concentrations observed across the district. There are no industrial activities of significance in the area apart from the economic activity of fishing and agriculture. Probable anthropogenic activities that may lead to fluoride enrichment include agricultural practices.

Nitrate levels are probably from oxidation of nitrogen from fertilizers (both inorganic and organic), oxidation of ammonia from animal waste and aerobic decomposition of nitrogenous organic matter. Animal husbandry is practiced in the area. In the rice growing area, probable source of NO_3^- is from fixing of nitrogen into the soil by rice roots which is in turn converted to nitrate via oxidation and fertilizer application. In the predominantly maize growing area, ammonia from animal waste and fertilizer applications are the sources. However, the levels did not violate any maximum allowable limit value. An inverse relationship between NO_3^- and Eh is apparent and with a significant correlation coefficient ($r = 0.558$, $p = 0.048$). This may suggest the important effect of Eh on NO_3^- evolution and possibly reduction of NO_3^- to NH_4^+ . But, this study did not include NH_4^+ determination. As such oxidation and reduction may be controlling levels of nitrate.

Redox sensitive elements

In PC3, Fe shows a direct relationship with turbidity and Mn_T with a mild positive loading of Al^{3+} included in this component. Thus, turbid waters in the area are due in part to presence of Fe_T and Mn_T . The color of particulates collected on the filter paper was consistent with presence of Fe_T . Solubility of metals decreases with pH (Mapoma et al. 2014) leading to precipitation and adsorption of iron, for instance. Although the correlation of Fe_T and pH is not that strong, Fe_T has a poor (but negative) relationship with SO_4^{2-} , HCO_3^- and Cl^- which are prime factors of pH changes. As such pH may be controlling the iron concentration besides availability of Fe-minerals in the aquifer. Dissolution of Fe-containing minerals (such as sulfides and silicates) can contribute to Fe_T concentrations observed. But poor relationship between Fe_T and SO_4^{2-} imply that sulfide minerals are not responsible for the iron present in the groundwater.

PHREEQC model shows that the groundwater is undersaturated with respect to melanterite (Fig. 7c) indicating that dissolution of this mineral plays a part in presence of iron. The supersaturation state of groundwater with respect to Fe-oxide minerals (hematite and magnetite) reduces the amount of dissolved Fe in the liquid phase while that of siderite (Fig. 7a) elevating Fe_T content. It was also observed that the saturation index of goethite was alternating between undersaturation and oversaturation states signifying that the changes in redox conditions, pH

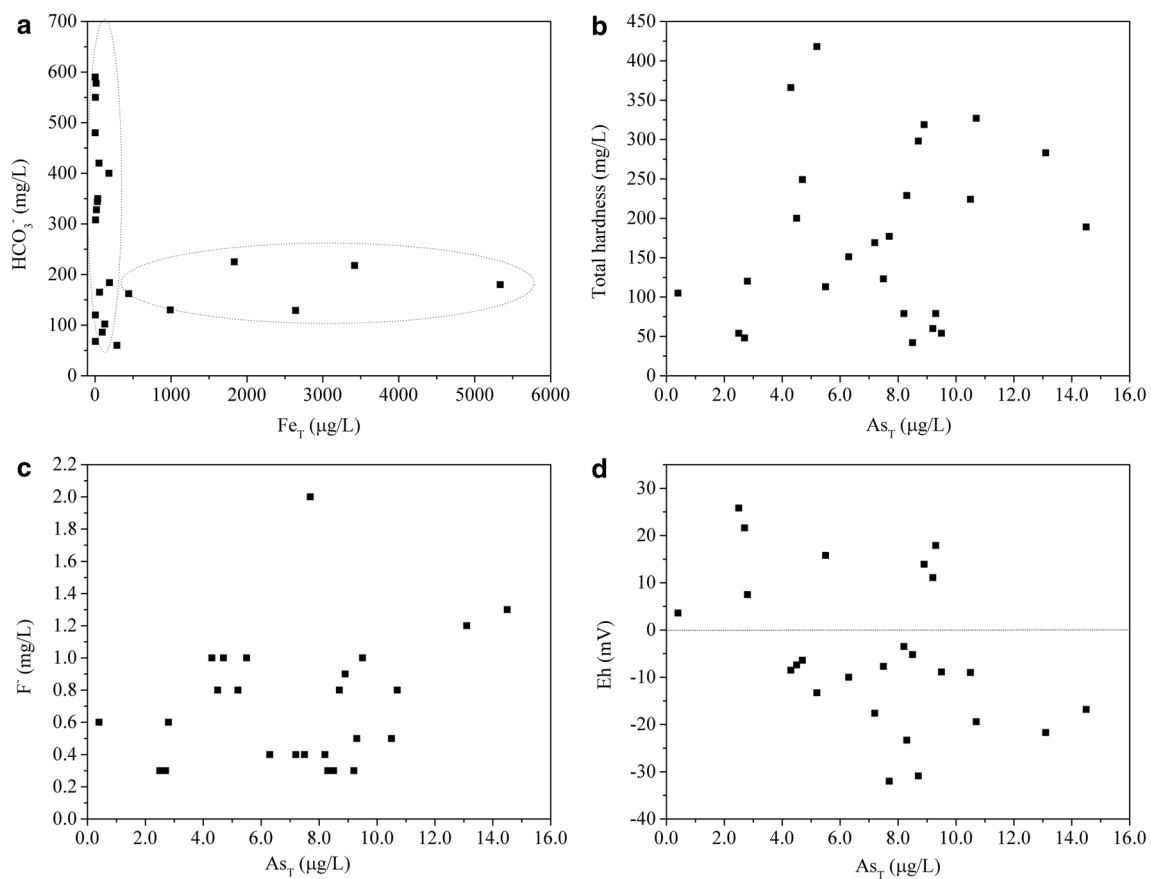


Fig. 8 Relationship between Fe_T and alkalinity (a), coexistence of As_T with TH (b) and F⁻ (c), and effect of Eh on As in the study area

and hydrolysis reactions affect localized levels of Fe_T in the groundwater. At low concentration of HCO₃⁻, Fe_T increases independent of alkalinity while siderite dissolution has little impact on HCO₃⁻ elevation as shown in Fig. 8a. Therefore, the main control of Fe_T content in groundwater samples studied is dissolution and precipitation mechanisms of Fe-containing minerals. Yet, the relationship with Mn_T, another redox sensitive element that controls Eh values, show that reduction/oxidation process has a role to play in Fe_T levels.

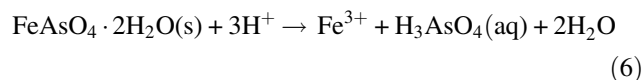
The speciation modeling with PHREEQC using the pH and Eh shows Fe(II) (predominantly as Fe²⁺) in the range of 3.65×10^{-8} – 9.28×10^{-5} mol/L while Fe(III) (as Fe(OH)²⁺) ranged from 8.88×10^{-13} to 1.42×10^{-9} mol/L. Compared to studies elsewhere in the country (Mapoma and Xie 2014), Fe_T in this area is low and below the WHO MALV (except for 16% of samples) probably due to seasonal fluctuations and formation of Fe-oxide solid phases (hematite and magnetite) and highly hydrated Fe-oxyhydroxides such as goethite (oversaturated index).

Manganese is positively related to turbidity and inversely correlated with K⁺ concentrations (Table 3). Here the factors further shows that the control on redox state by Mn_T can have an effect on levels of K⁺ from silicate dissolution

or cation exchange. About 32% of samples (*n* = 25) exceed the desired 400 μg/L Mn_T in drinking water (WHO 2011). The areas with high manganese content are expected to show higher values of turbidity. However, only 56% of the samples showed values of turbidity above 0 NTU (Table 1). But these are the samples whose Mn_T content exceeded WHO (2011) limit value contributing 28% to the observed violation. Reductive dissolution of manganite is one of the sources of manganese in the system (Fig. 7e).

The samples where As_T values exceed 10 μg/L were found in groundwater with higher total hardness (as CaCO₃, mg/L) and fluoride (Fig. 8b, c). Of course this assessment has not been done in the study area before, but it suggests that hard water in the rice growing region of Karonga may contain higher than WHO limit value of As and that areas with hard water and high F⁻ content are synonymous with arsenic enrichment. This equally applies to areas with generally high TDS (*r* = 0.933, *p* < 0.001). The regression analysis shows that As_T is significantly related to the evolution of pH (*r* = 0.369, *p* = 0.035) and HCO₃⁻ (*r* = 0.351, *p* = 0.043). From Fig. 8d, it shows that higher arsenic content was observed in relatively reducing conditions than oxidizing conditions although the Eh values of groundwater are relatively low compared to

those observed in arsenic laden aquifers across the globe. Possibly, this is suggesting that As is mobilized by the changes in redox conditions of groundwater coupled to other mechanisms such as rock–water interaction and pH leading to dissolution of As-containing minerals, e.g., arsenolite (Eq. 5) and pH dependent dissolution of As-containing Fe-minerals, e.g., scorodite (Eq. 6).



In this study, arsenolite was found to be undersaturated with respect to the liquid phase ($\text{SI}_{\text{mean}} = -25.9$).

Siderite is an effective sink of arsenic released in shallow groundwater as that of Karonga aquifer (Mumford et al. 2012). Although the binding of As(III) to siderite is weak, it is still a good sequestrant of arsenic in groundwater especially for As(V). However, siderite was undersaturated in this study. As shown earlier, goethite and Fe-oxides were precipitating that may sequester the already low concentration of As_T present in the system while dissolution of oxyhydroxides/hydroxides (Fig. 7e, f) can release arsenic held in the mineral matrix. It was modeled using PHREEQC that As(III) (5.18×10^{-9} – 1.84×10^{-7} mol/L) was predominated by $\text{H}_3\text{AsO}_3(\text{aq})$ while As(V) (1.60×10^{-10} – 4.53×10^{-8} mol/L) existed mostly as H_2AsO_4^- and HAsO_4^{2-} . The predominance of As(III) over As(V) is crucial to the overall determination of the detrimental effect of contaminated groundwater used for drinking since As(III) is more toxic and more mobile than As(V) which adsorbs strongly to surface complexes (Charlet et al. 2007).

Conclusions

Higher values of alkalinity (as HCO_3^-), Fe_T , Mn_T and As_T were observed in some samples while sample KA-05 showed F^- value greater than 1.5 mg/L WHO standard. Furthermore, low concentration of NO_3^- (48% non-detects) was observed. The overall index (WQI) showed that 36% of samples were very poor while 16% of the samples were rated as unfit for drinking. Sample KA-04 showed a high salinity hazard and low sodium adsorption ratio (SAR) which is not ideal for soils with limited drainage. Carbonate dissolution, silicate weathering and cation exchange are suggested as main hydrochemical mechanisms constrained by slightly acidic to neutral pH and reducing conditions. The possible sources of F^- could be anthropogenic and rock–water interaction in this Karonga aquifer. Although the concentrations of As_T , F^- , Fe_T , Mn_T and NO_3^- were low (except where the values

exceeded the WHO standards), constant assessment and monitoring of groundwater is needed in this aquifer to safeguard the health of the communities using this aquifer.

Acknowledgements This study received material support from University of Malawi. Mr. A Maliro and Mr. D. Chimutu assisted in sampling and field data collection. Colleagues from the Department of Water in Karonga district, Malawi assisted greatly during sampling work. This research was financially supported by the National Natural Science Foundation of China (Nos. 41521001, 41372254 and 41202168).

References

- Allison JD, Brown DS, Kevin J (1991) MINTEQA2/PRODEFA2, a geochemical assessment model for environmental systems: Version 3.0 user's manual. Environmental Research Laboratory, Office of Research and Development, US Environmental Protection Agency Athens, GA
- Asadi S, Vuppala P, Reddy MA (2007) Remote sensing and GIS techniques for evaluation of groundwater quality in municipal corporation of Hyderabad (Zone-V), India. *Int J Environ Res Public Health* 4:45–52. doi:10.3390/ijerph2007010008
- Ayedun H, Taiwo A, Umar B, Oseni O, Oderinde A (2011) Assessment of groundwater contamination by toxic metals in Ifo, Southwestern Nigeria. *Indian J Sci Technol* 4:820–823. doi:10.17485/ijst/2011/v4i7/30118
- Bhattacharya S, Gupta K, Debnath S, Ghosh UC, Chattopadhyay D, Mukhopadhyay A (2012) Arsenic bioaccumulation in rice and edible plants and subsequent transmission through food chain in Bengal basin: a review of the perspectives for environmental health. *Toxicol Environ Chem* 94:429–441
- Burton ED, Johnston SG, Kraal P, Bush RT, Claff S (2013a) Sulfate availability drives divergent evolution of arsenic speciation during microbially mediated reductive transformation of schertmannite. *Environ Sci Technol* 47:2221–2229. doi:10.1021/es303867t
- Burton ED, Johnston SG, Planer-Friedrich B (2013b) Coupling of arsenic mobility to sulfur transformations during microbial sulfate reduction in the presence and absence of humic acid. *Chem Geol* 343:12–24. doi:10.1016/j.chemgeo.2013.02.005
- Carter G, Bennett JD (1973) Geology and mineral resources of Malawi. *Malawi Geol Surv Dep Bull* 6:1–62
- Charlet L, Chakraborty S, Appelo CAJ, Roman-Ross G, Nath B, Ansari AA, Lanson M, Chatterjee D, Mallik SB (2007) Chemodynamics of an arsenic “hotspot” in a West Bengal aquifer: a field and reactive transport modeling study. *Appl Geochem* 22:1273–1292. doi:10.1016/j.apgeochem.2006.12.022
- Chilton PJ, Smith-Carington AK (1984) Characteristics of the weathered basement aquifer in Malawi in relation to rural water supplies. In: Walling DE, Foster SSD, Wurzel P (eds) Proceedings of the Harare symposium. IAHS Publ no 144, Harare, pp 57–72
- Chimpamba J, Ngongondo C, Mleta P (2009) Groundwater chemistry of basement aquifers: a case study of Malawi. In: Titus R, Beekman H, Adams S, Strachan L (eds) Basement aquifers of Southern Africa, WRC report no TT 428-09. Water Research Commission
- Dill H, Ludwig R-R, Kathewera A, Mwenelupembe J (2005) A lithofacies terrain model for the Blantyre Region: implications for the interpretation of palaeosavanna depositional systems and for environmental geology and economic geology in southern

- Malawi. *J Afr Earth Sci* 41:341–393. doi:[10.1016/j.jafrearsci.2005.07.005](https://doi.org/10.1016/j.jafrearsci.2005.07.005)
- Etteieb S, Cherif S, Tarhouni J (2015) Hydrochemical assessment of water quality for irrigation: a case study of the Medjerda River in Tunisia. *Appl Water Sci*. doi:[10.1007/s13201-015-0265-3](https://doi.org/10.1007/s13201-015-0265-3)
- Fagereng Å (2013) Fault segmentation, deep rift earthquakes and crustal rheology: insights from the 2009 Karonga sequence and seismicity in the Rukwa–Malawi rift zone. *Tectonophysics* 601:216–225. doi:[10.1016/j.tecto.2013.05.012](https://doi.org/10.1016/j.tecto.2013.05.012)
- Gomez M, Blarasin M, Martínez D (2009) Arsenic and fluoride in a loess aquifer in the central area of Argentina. *Environ Geol* 57:143–155. doi:[10.1007/s00254-008-1290-4](https://doi.org/10.1007/s00254-008-1290-4)
- Halim MA, Majumder RK, Nessa SA, Hiroshiro Y, Sasaki K, Saha BB, Saepuloh A, Jinno K (2010) Evaluation of processes controlling the geochemical constituents in deep groundwater in Bangladesh: spatial variability on arsenic and boron enrichment. *J Hazard Mater* 180:50–62. doi:[10.1016/j.jhazmat.2010.01.008](https://doi.org/10.1016/j.jhazmat.2010.01.008)
- Kortatsi BK, Tay CK, Anornu G, Hayford E, Dartey GA (2008) Hydrogeochemical evaluation of groundwater in the lower Offin basin, Ghana. *Environ Geol* 53:1651–1662. doi:[10.1007/s00254-007-0772-0](https://doi.org/10.1007/s00254-007-0772-0)
- Macheyeki AS, Mdala H, Chapola LS, Manhiça VJ, Chisambi J, Feitio P, Ayele A, Barongo J, Ferdinand RW, Ogubazghi G, Goitom B, Hlatywayo JD, Kianji GK, Marobhe I, Mulowezi A, Mutamina D, Mwano JM, Shumba B, Tumwikirize I (2015) Active fault mapping in Karonga–Malawi after the December 19, 2009 Ms 6.2 seismic event. *J Afr Earth Sci* 102:233–246. doi:[10.1016/j.jafrearsci.2014.10.010](https://doi.org/10.1016/j.jafrearsci.2014.10.010)
- Mapoma HWT, Xie X (2014) Basement and alluvial aquifers of Malawi: an overview of groundwater quality and policies. *African J Environ Sci Technol* 8:190–202. doi:[10.5897/ajest2013.1639](https://doi.org/10.5897/ajest2013.1639)
- Mapoma HWT, Xie X, Zhang L (2014) Redox control on trace element geochemistry and provenance of groundwater in fractured basement of Blantyre, Malawi. *J Afr Earth Sci* 100:335–345. doi:[10.1016/j.jafrearsci.2014.07.010](https://doi.org/10.1016/j.jafrearsci.2014.07.010)
- Merkel BJ, Planer-Friedrich B (2005) Groundwater geochemistry: a practical guide to modeling of natural and contaminated aquatic systems. Springer, Berlin
- Mkandawire T (2008) Quality of groundwater from shallow wells of selected villages in Blantyre District, Malawi. *Phys Chem Earth Parts A/B/C* 33:807–811. doi:[10.1016/j.pce.2008.06.023](https://doi.org/10.1016/j.pce.2008.06.023)
- Monjerezi M, Ngongondo C (2012) Quality of groundwater resources in Chikhwawa, Lower Shire Valley, Malawi. *Water Qual Expo Health* 4:39–53. doi:[10.1007/s12403-012-0064-0](https://doi.org/10.1007/s12403-012-0064-0)
- Monjerezi M, Vogt RD, Aagaard P, Gebru AG, Saka JD (2011) Using $^{87}\text{Sr}/^{86}\text{Sr}$, $\delta^{18}\text{O}$ and $\delta^2\text{H}$ isotopes along with major chemical composition to assess groundwater salinization in lower Shire valley, Malawi. *Appl Geochem* 26:2201–2214. doi:[10.1016/j.apgeochem.2011.08.003](https://doi.org/10.1016/j.apgeochem.2011.08.003)
- MSB (2005) Borehole and shallow well water quality—specification, MS 733:2005. Malawi Standards Board, Blantyre
- Mukherjee A, Fryar AE (2008) Deeper groundwater chemistry and geochemical modeling of the arsenic affected western Bengal basin, West Bengal, India. *Appl Geochem* 23:863–894. doi:[10.1016/j.apgeochem.2007.07.011](https://doi.org/10.1016/j.apgeochem.2007.07.011)
- Mukherjee A, Fryar AE, Thomas WA (2009) Geologic, geomorphic and hydrologic framework and evolution of the Bengal basin, India and Bangladesh. *J Asian Earth Sci* 34:227–244. doi:[10.1016/j.jseaes.2008.05.011](https://doi.org/10.1016/j.jseaes.2008.05.011)
- Mumford AC, Barringer JL, Benzel WM, Reilly PA, Young L (2012) Microbial transformations of arsenic: mobilization from glauconitic sediments to water. *Water Res* 46:2859–2868. doi:[10.1016/j.watres.2012.02.044](https://doi.org/10.1016/j.watres.2012.02.044)
- O'Neill A, Phillips DH, Kok S, Chea E, Seng B, Sen Gupta B (2013) Arsenic in groundwater and its influence on exposure risks through traditionally cooked rice in Prey Veng Province, Cambodia. *J Hazard Mater* 262:1072–1079. doi:[10.1016/j.jhazmat.2013.03.063](https://doi.org/10.1016/j.jhazmat.2013.03.063)
- Parkhurst DL, Appelo CAJ (1999) User'S Guide to Phreeqc (Version 2)—a computer program for speciation, batch-reaction, one-dimensional transport, and inverse geochemical calculation. US Geological Survey, Denver
- Pradhan S, Patnaik D, Rout S (2001) Water Quality Index for the groundwater around a phosphatic fertilizer plant. *Indian J Environ Prot* 21:355–358
- Rafique T, Naseem S, Bhanger MI, Usmani TH (2008) Fluoride ion contamination in the groundwater of Mithi sub-district, the Thar Desert, Pakistan. *Environ Geol* 56:317–326. doi:[10.1007/s00254-007-1167-y](https://doi.org/10.1007/s00254-007-1167-y)
- Rafique T, Naseem S, Usmani TH, Bashir E, Khan FA, Bhanger MI (2009) Geochemical factors controlling the occurrence of high fluoride groundwater in the Nagar Parkar area, Sindh, Pakistan. *J Hazard Mater* 171:424–430. doi:[10.1016/j.jhazmat.2009.06.018](https://doi.org/10.1016/j.jhazmat.2009.06.018)
- Rahmanian N, Ali SHB, Homayoonfard M, Ali NJ, Rehan M, Sadef Y, Nizami AS (2015) Analysis of physiochemical parameters to evaluate the drinking water quality in the State of Perak, Malaysia. *J Chem* 2015:1–10. doi:[10.1155/2015/716125](https://doi.org/10.1155/2015/716125)
- Rice EW, Baird RB, Eaton AD, Clesceri LS (eds) (2012) Standard methods for the examination of water and wastewater, 22nd edn. American Public Health Association, American Water Works Association, Water Environment Federation, Washington
- Singh KP, Malik A, Mohan D, Singh VK, Sinha S (2006) Evaluation of groundwater quality in northern Indo-Gangetic alluvium region. *Environ Monit Assess* 112:211–230. doi:[10.1007/s10661-006-0357-5](https://doi.org/10.1007/s10661-006-0357-5)
- Smedley P, Kinniburgh D (2002) A review of the source, behaviour and distribution of arsenic in natural waters. *Appl Geochem* 17:517–568. doi:[10.1016/S0883-2927\(02\)00018-5](https://doi.org/10.1016/S0883-2927(02)00018-5)
- Srivastava P, Mukherjee S, Gupta M, Singh S (2011) Characterizing monsoon variation on water quality index of River Mahi in India using geographical information system. *Water Qual Expo Health* 2:193–203. doi:[10.1007/s12403-011-0038-7](https://doi.org/10.1007/s12403-011-0038-7)
- Stephens EA (1966) Geological account of the northwest coast of Lake Malawi between Karonga and Lion Point, Malawi. *Am Anthropol* 68:50–58. doi:[10.1525/aa.1966.68.2.02a00970](https://doi.org/10.1525/aa.1966.68.2.02a00970)
- Sun G-X, Williams PN, Carey A-M, Zhu Y-G, Deacon C, Raab A, Feldmann J, Islam RM, Meharg AA (2008) Inorganic arsenic in rice bran and its products are an order of magnitude higher than in bulk grain. *Environ Sci Technol* 42:7542–7546. doi:[10.1021/es801238p](https://doi.org/10.1021/es801238p)
- Thompson JC, Mackay A, Wright DK, Welling M, Greaves A, Gomani-Chindebvu E, Simengwa D (2012) Renewed investigations into the Middle Stone Age of northern Malawi. *Quat Int* 270:129–139. doi:[10.1016/j.quaint.2011.12.014](https://doi.org/10.1016/j.quaint.2011.12.014)
- Tiwari T, Mishra M (1985) A preliminary assignment of water quality index of major Indian rivers. *Indian J Environ Prot* 5:276–279
- Wanda E, Monjerezi M, Mwatseteza JF, Kazembe LN (2011) Hydro-geochemical appraisal of groundwater quality from weathered basement aquifers in Northern Malawi. *Phys Chem Earth Parts A/B/C* 36:1197–1207. doi:[10.1016/j.pce.2011.07.061](https://doi.org/10.1016/j.pce.2011.07.061)
- Wanda EMM, Gulula LC, Phiri A (2013) Hydrochemical assessment of groundwater used for irrigation in Rumphu and Karonga districts, Northern Malawi. *Phys Chem Earth Parts A/B/C* 66:51–59. doi:[10.1016/j.pce.2013.09.001](https://doi.org/10.1016/j.pce.2013.09.001)
- Wang Y, Guo H, Yan S, Wang R, Li Y (2004) Geochemical evolution of shallow groundwater systems and their vulnerability to contaminants: a case study at Datong Basin, Shanxi province, China. Science Press, Beijing
- Wang Y, Shvartsev SL, Su C (2009) Genesis of arsenic/fluoride-enriched soda water: a case study at Datong, northern China.

- Appl Geochem 24:641–649. doi:[10.1016/j.apgeochem.2008.12.015](https://doi.org/10.1016/j.apgeochem.2008.12.015)
- WHO (2011) Guidelines for drinking-water quality, 4th edn. World Health Organization, Geneva
- Wright DK, Thompson J, Mackay A, Welling M, Forman SL, Price G, Zhao J-x, Cohen AS, Malijani O, Gomani-Chindebvu E (2014) Renewed geoarchaeological investigations of mwan-ganda's village (elephant butchery site), Karonga, Malawi. *Geoarchaeology* 29:98–120. doi:[10.1002/gea.21469](https://doi.org/10.1002/gea.21469)
- Yidana SM (2010) Groundwater classification using multivariate statistical methods: Birimian Basin, Ghana. *J Environ Eng* 136:1379–1388. doi:[10.1061/\(ASCE\)EE.1943-7870.0000291](https://doi.org/10.1061/(ASCE)EE.1943-7870.0000291)
- Zouahri A, Dakak H, Douaik A, El Khadir M, Moussadek R (2015) Evaluation of groundwater suitability for irrigation in the Skhirat region, Northwest of Morocco. *Environ Monit Assess* 187:4184. doi:[10.1007/s10661-014-4184-9](https://doi.org/10.1007/s10661-014-4184-9)